Effect of Al2O3 ALD coating on thermal stability of silica aerogel

Effect of Al_2O_3 ALD Coating on Thermal Stability of Silica Aerogel

Sungwoo Yang [†], Elise Strobach, David Bierman [‡], Lin Zhao, Bikram Bhatia and Evelyn N. Wang *

Department of Mechanical Engineering, Massachusetts Institute of Technology, Cambridge, Massachusetts 02139, USA

[†] *Current position: Department of Chemical Engineering, University of Tennessee Chattanooga, Chattanooga, Tennessee 37403, USA*

[‡] *Current position: Antora Energy*

HIGHLIGHTS

Enhanced thermal stability of transparent silica aerogel via Al_2O_3 ALD coating

Optimization of Al_2O_3 ALD needed to balance transmission and thermal properties

ABSTRACT

An optically transparent and thermally insulating (OTTI) silica aerogel demonstrates promising results for various solar thermal applications, particularly concentrated solar power systems. Higher system efficiency can be achieved by integrating OTTI materials by reducing heat loss at higher receiver temperature. However, the thermal stability of OTTI aerogels has been one of the limiting factors. Here, we report that Al_2O_3 atomic layer deposition (ALD) enhances the thermal stability of silica aerogel. The more layers of Al_2O_3 ALD coating on silica aerogels, the higher the thermal stability. However, more layers of Al_2O_3 ALD coating compromises transmittance of silica aerogel due to increasing the size of scattering centers. Therefore, optimization of Al_2O_3 ALD coating needs to be performed to enhance performance for a solar thermal system. The demonstrated ALD-coated aerogel provides a potential pathway to further improve the efficiency and reduce the cost of state-of-the-art concentrating solar power (CSP) systems.

* Corresponding author. Tel.: +1 6173243311.
E-mail address: enwang@mit.edu (E.N. Wang).

KEYWORDS: Optically transparent thermally insulating silica aerogel, atomic layer deposition, solar-thermal energy conversion, concentrated solar power

1. INTRODUCTION

Global annual energy consumption is equivalent to one-hour solar irradiation on Earth.[1] This abundance makes solar energy a promising renewable energy source. Solar energy can be converted into electricity via photovoltaic (PV) cells or into useful thermal energy via concentrating solar power (CSP). CSP systems collect solar radiation onto an absorbing receiver to generate usable thermal energy. While PV is the dominant solar energy conversion technology, CSP promises low-cost and high-efficiency thermal storage that can provide energy throughout a 24-hour cycle.[2] However, the cost of electricity generated using CSP is still limited by low overall efficiency. As higher operating temperatures of the CSP receiver and power cycles are achieved, a significant increase in overall efficiency is possible by enabling the use of power towers for solar collection and supercritical CO_2 cycles for electricity generation.[3] However, it is critical to minimize thermal losses at these high temperatures to realize high-efficiency solar collection and electricity generation using CSP. Optically transparent and thermally insulating silica aerogel can help reduce heat loss from the high-temperature receivers substantially and significantly improve CSP efficiency with minimal cost impact or design change.[4,5]

Silica aerogel is an optically transparent and thermally insulating porous material. Its unique nanoporous structure allows a large fraction of solar irradiation to travel through the aerogel, resulting in high transmittance while suppressing solid conduction, gas phase convection, and infrared radiation (IR). The combination of both high transmittance and low thermal conductivity is extremely rare in nature, which makes silica aerogel a promising candidate for various solar related applications including solar thermal

converters and efficient building windows.[6–10] However, despite the advantages of superior optical and thermal properties of silica aerogel, its solar related applications remain limited due to the lack of thermal stability of silica aerogel. A general shrinkage of pores and overall volume is attributed to the condensation reaction and structural relaxation above the critical temperature (~400 °C).[11] As temperature increases, the viscosity of the aerogel particles decreases, which results in irreversible particle aggregation and densification.[12] Consequently, changes in pores, particles and overall volume have a significant effect on the optical and thermal properties of the aerogel. While studies have shown that silica aerogel annealed up to 600 °C will reach a steady-state nanostructure within 30 days of continuous annealing, the material still shows shrinkage around 10 % in length before reaching a stable end-point.[13] Therefore, the deployment of traditional silica aerogel requires careful consideration for application at high temperatures, and has been limited in use due to thermal stability related concerns.

In this work, we demonstrate enhanced thermal stability of transparent silica aerogel by Al_2O_3 atomic layer deposition (ALD). Noticeable structural change on Al_2O_3 ALD coated aerogel was observed at and above 700 °C. The more layers of Al_2O_3 ALD coating on silica aerogels, the higher thermal stability. However, these layers of Al_2O_3 ALD coating reduced solar transmittance of silica aerogel due to increasing the size of scattering centers. Both operating temperature and transmittance are important factors in determining the receiver efficiency. Therefore, we optimized the Al_2O_3 ALD coating to enable the best performance of solar thermal systems. The development of high temperature stable aerogel promises new applications that require high transparency and thermal insulation, such as transparent doors of high-temperature furnaces/ovens, transparent insulation for certain sections of tubes that carry high-temperature fluid and space shuttle cockpit windows.

2. EXPERIMENTAL

We synthesized transparent silica aerogel using conventional metal-alkoxide polymerization. Hydrolysis reaction and condensation reactions are key to controlling the particle and pore size of the aerogel. To obtain highly transparent aerogel, small and uniformly distributed particles and pore sizes are preferred. Tetramethyl orthosilicate (TMOS, 131903, Sigma Aldrich) was used as the silica precursor. To control both the hydrolysis and condensation reaction rate, an ammonia solution (NH_3, 2.0 M in methanol, 341428, Sigma Aldrich) was used as the catalyst. TMOS was diluted with methanol (MeOH, 322415, Sigma Aldrich) since it does not react with TMOS and ensures suitable miscibility with water. The diluted TMOS solution was mixed with NH_3 and water. Our optimized chemical ratio to synthesize OTTI silica aerogel was NH_3:TMOS:water:methanol = 0.004:1:4:6.[14] The mixed solution was placed in a transparent container. Upon the completion of gelation (~5 minutes), the gel was aged at various temperature (25, 40, 50 and 60 °C) for various aging time (1, 3, 5, 7 and 14 days) to strengthen the silica backbone network within the gel. After aging, the mother solvent, mostly MeOH and water, was replaced with ethanol (EtOH, 89234-848, VWR) as it is miscible with liquid CO_2. The conventional critical point drying (CPD, model 931, Tousimis) method was used to dry the wet gels. Decreasing capillary pressure during the CPD process is the key to minimize cracks of the aerogels. Therefore, we used a minimal bleed rate at 100 psi/hr to decrease the CPD chamber pressure from ~ 1300 psi to ambient pressure. Al_2O_3 ALD on synthesized silica aerogel was performed on a F200, Cambridge Nanotech Fiji. The aerogels were mounted on an 4 inch Si(001) wafer and then heated to 250 °C with N_2 flow rate at 20 sccm. The two half-reaction steps consisted of injecting desired times H_2O or $Al(CH_3)_3$ (trimethylaluminum (TMA)). To complete a cycle of Al_2O_3 coating, 8 times of 0.03 s H_2O pulse and 1.5 s purge were applied, followed by 8 times of 0.09 s TMA pulse and 3 s purge. ALD growth cycles of 10, 25, 50 and 100 were used to prepare the Al_2O_3 coated silica aerogels. After the initial characterizations including small angle x-ray scattering

(SAXS) and UV-vis NIR, the samples were placed in an oven for annealing to examine the thermal stability of the samples at desired temperature. Temperature ramping rate was 10 °C/min. Upon the completion of annealing, we carefully removed the sample from the oven and placed it in a ceramic dish to cool to room temperature. The annealed samples were re-characterized to monitor optical and structural changes after the annealing process. We used image analysis (ImageJ software) to measure the dimensions of aerogels before and after the annealing process.[15] Adsorption-desorption isotherms for nitrogen at 77 K were aquired by a surface analyzer (NOVA Touch LX2, Quantachrome). The specific surface area and pore size distribution of the solid were based on the multipoint Brunner-Emmett-Teller theory (BET) and nonlocal density functional theory (NLDFT). We measured the total hemispherical transmittance (250~2500 nm) of the samples using a spectrometer (Cary 5000 UV-vis NIR, Agilent). The scattering length distribution and the average scattering radius size were characterized by using small angle x-ray scattering (SAXSLAB instrument) with a Cu K-alpha x-ray source. To ensure the best fit of the transmission and reflection data, we probed the center of the synthesized aerogels. This technique reduced edge defect effects and maintained measurement integrity. We used SAXSGUI software to deduce the scattering patterns and used MCSAS software to estimate the mean scattering radius.[16,17]

3. RESULTS AND DISCUSSION

3.1 The shrinkage of aerogel

We optimized the synthetic recipe to produce large transparent aerogel (~130 cm^2) without noticeable cracks as shown in Figure 1a. Minimizing mechanical stress during the synthesis was the key to minimize the cracks. Its solar-weighted transmittance was measured to be approximately 96% at 8 mm thickness, which is higher than that of glass (~ 92%) as shown in Figure 1b. The extraordinary high transmittance of

silica aerogel was due to the low extinction in the solar band resulting from scattering in the visible and ultraviolet wavelengths.[14] Since the scattering coefficient is proportional to the third power of the diameter of the scattering centers (i.e., combination of particles and pores), keeping uniform and minimal sizes of similar particles and pores is critical.[18] The synthesized silica aerogel demonstrated narrow pore size distribution (d_p = ~8.4 nm in Figure 1c), uniform pores (inserted SEM image in Figure 1c) and particles (TEM image in Figure 1d). The resulting wavelengths exhibited weak scattering in the shorter bands.

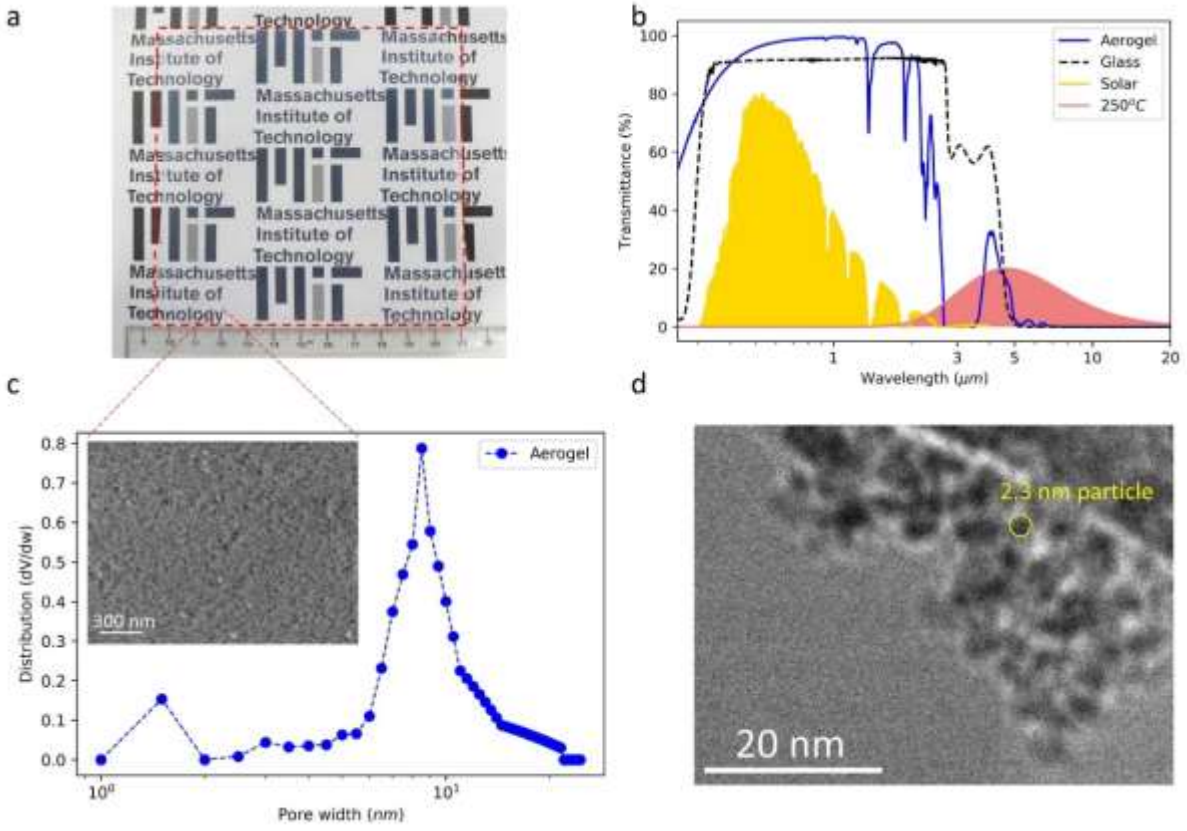

Figure 1. (a) Image of a transparent silica aerogel (thickness: 8 mm, area: ~130 cm^2). (b) Direct-hemispherical transmittance spectrum (blue solid) of an 8 mm thick aerogel sample measured by a UV–vis–NIR spectrophotometer and an FTIR spectrometer. Transmittance of the soda-lime glass slide at 2 mm thickness (black dotted) is also shown for comparison. Sharp peaks in the aerogel spectrum between 1 and 3 μm originate from absorption by water molecules and silanol groups present on the surface of silica particles. (c) Pore size distribution based on N_2 adsorption-desorption isotherm. Insets: SEM images of a transparent aerogel. (d) TEM image of a transparent aerogel showing its particle size of ~2.3 nm particle.

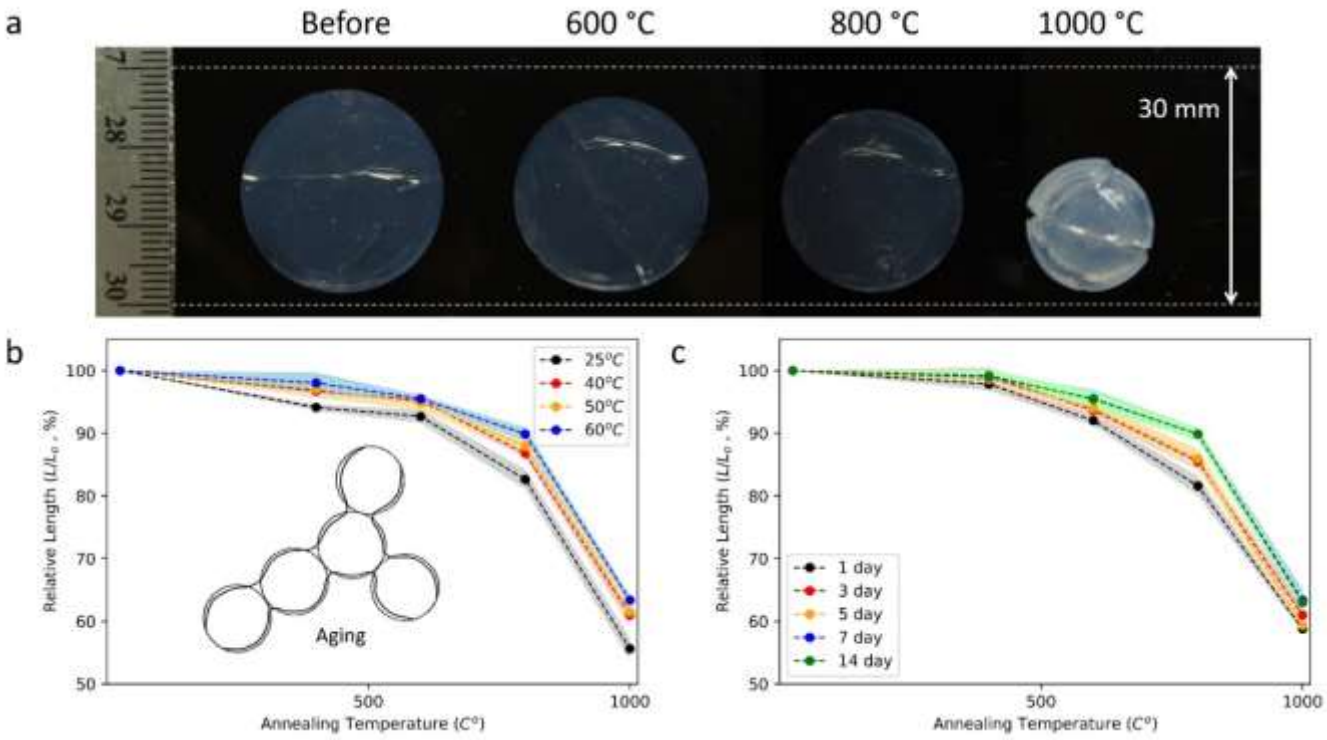

Figure 2. (a) Images of silica aerogel before and after annealing at 600, 800 and 1000 °C. (b) Relative length shrinkage of aerogel aged at various temperatures (25, 40, 50 and 60 °C in black, red, yellow and blue, respectively) as annealed between 400 and 1000 °C for 1 day. (c) Relative length shrinkage of aerogel aged at 60 °C for various time (1, 3, 5, 7 and 14 days in black, red, yellow and blue, respectively) as annealed between 400 and 1000 °C for 1 day.

However, as shown in Figure 2a, the silica aerogel shrinks as a result of the condensation reaction and structural relaxation above ~ 400 °C, which limits its use for high-temperature applications. High temperature exposure decreases the viscosity of the silica particles resulting in a change in size of both particle and pores of silica porous network. To strengthen the gel network and minimize the shrinkage, aging conditions including aging temperature and period were optimized. During the aging of the gel, a process of dissolution and reprecipitation, called coarsening, causes growth of necks between particles, increasing strength and stiffness of the gel.[19] Differences in solubility between surfaces with different radii

of silica particle curvature drives the coarsening process which is a function of the aging temperature.[20,21] We synthesized multiple silica aerogel using the optimized chemical ratio mentioned in the experimental section above. Wet silica gels were prepared in small plastic vials (~1 inch). The gels were aged at various temperature between 25 °C and 60 °C for 24 hours and various aging times between 1 day to 14 days at 60 °C, followed by solvent exchange and drying. Figure 2b and 2c show the relative length measurement results annealed at various temperature from 400 °C to 1000 °C for 24 hours. The x-axis shows annealing temperature, and y-axis shows relative length change (L/L_0) where L and L_0 is the length of aerogel after and before the annealing. The relative length is the average of the measured results, and the error (shown by the shaded regions) was based on the standard deviation of the measurements. The results demonstrate that the higher aging temperature and the longer aging time, the less shrinkage due to increasing strength and stiffness of the gel. No further noticeable enhancement was observed after 14 days. In addition, 60 °C was the highest aging temperature since the boiling temperature of methanol, which is the major solvent of the initial solution, is 64.7 °C. Therefore, the Al_2O_3 ALD coating was applied to aerogels aged at 60 °C for 14 days to maximize the strength of the silica network.

We synthesized a large monolithic aerogel (similar to the one in Figure 1a) with the optimized aging process. We used a laser cutter (Zing 24 Laser, Epilog) to obtain identical silica aerogel samples prior to Al_2O_3 ALD coating. Figure 3a shows images of silica aerogel samples (< 4 cm^2) before and after Al_2O_3 ALD coatings at 10, 25, 50 and 100 cycles. For the samples with ALD coatings at 10 and 25 cycles, there was no significant change in the visual appearance of the Al_2O_3 coated samples. For the samples with ALD coatings at 50 and 100 cycles, more cracks and less transparency became noticeable. Figure 3b shows images of pristine and Al_2O_3 coated silica aerogels after annealing at 600℃ for 14 days. While there was shrinkage in the pristine silica aerogel, the Al_2O_3 coated silica aerogels showed negligible shrinkage after the annealing. The annealing process between 400℃~ 600 ˚C caused stress to release and

a phase transition resulting in a decrease in refractive index of the coated Al_2O thin film.[22] Consequently, as shown in Figure 3b, we observed that the transmitance of the Al_2O_3 coated silica aerogel increased after annealing at 600℃.

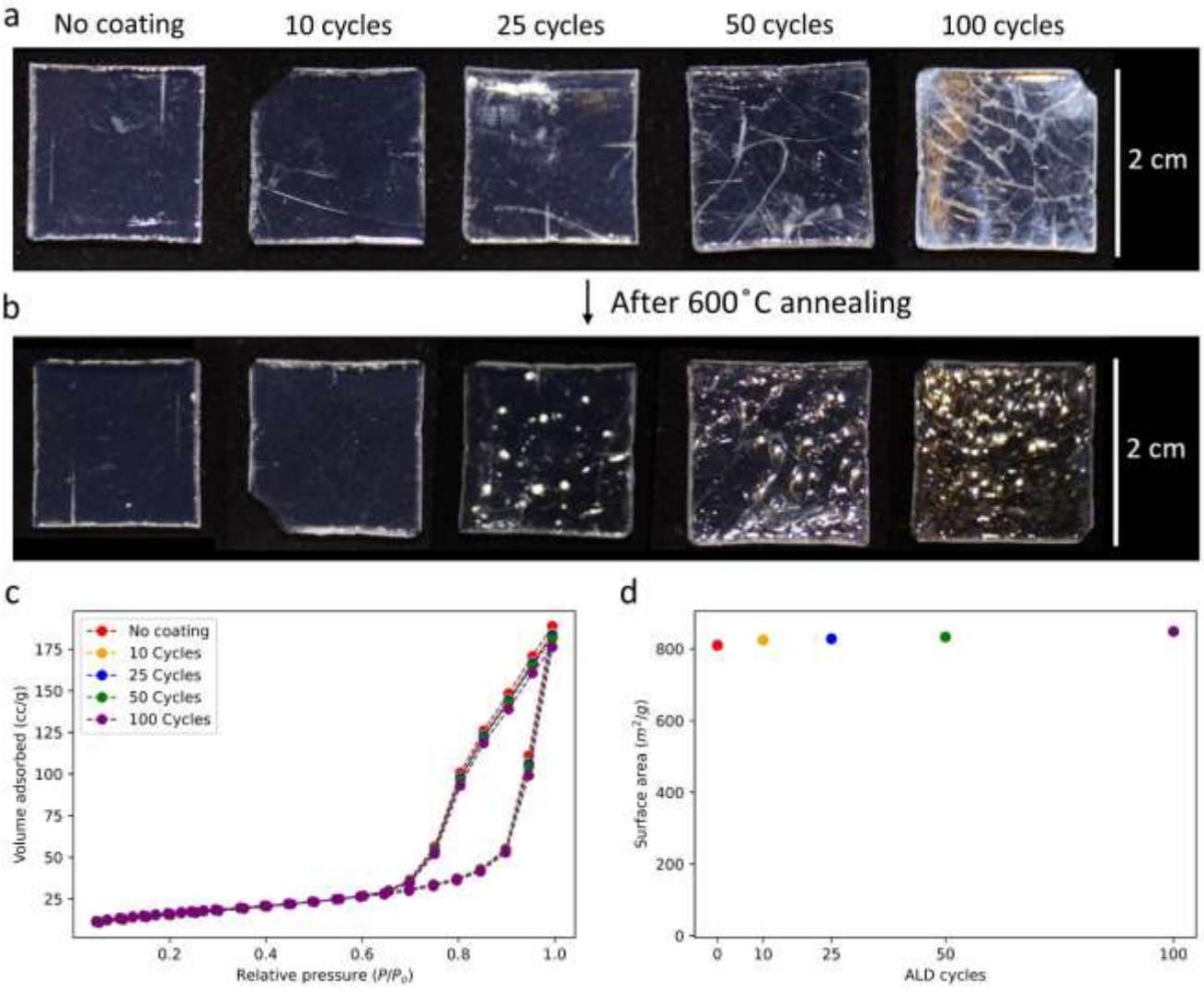

Figure 3. (a) Images of silica aerogel before and after Al_2O_3 ALD coatings at 0, 10, 25, 50 and 100 cycles. The scale bar is 2 cm. (b) Images of pristine and Al_2O_3 coated silica aerogels after annealing at 600℃. (c) N_2 adsorption-desorption isotherms of the aerogel with and without Al_2O_3 ALD coatings (0, 10, 25, 50 and 100 ALD cycles in red, yellow, blue, green and purple, respectively). (d) Multipoint BET surface area analysis of the aerogel over ALD cycles.

The N_2 adsorption-desorption isotherms of pristine and Al_2O_3 coated aerogels are shown in Figure 3c. All isotherms were type IV which indicates that the mesopores did not change after the Al_2O_3 ALD coating. In addition, the BET specific surface area of the coated samples were estimated using the multipoint BET method (Figure 3d). It demonstrated that the surface area of the coated samples remained relatively constant even after the Al_2O_3 ALD coating. The Al_2O_3 coating can affect surface area by filling the pores of hirachical porous structure which decreases the surface area or it can thicken the primary silica particles whichs results in an increase in surface area. The relatively unaffected surface area suggests that both effects were not significant and the pores of the samples stayed open during the Al_2O_3 ALD coating.

3.2 Enhanced thermal stability

Figure 4a shows the relative length change over various annealing temperatures (25 °C, 400 °C, 600 °C, 800 °C and 1000 °C) for 14 days. As-synthesized silica aerogels showed noticeable shrinkage as a result of the condensation reaction and structural relaxation above ~ 400 °C. On the other hand, silica aerogel with Al_2O_3 ALD coating did not show visible shrinkage up to ~ 600 °C for 14 days. Negligible shrinkage of aerogels annealed less than 600 °C is attributed to minimal pore radius change. In addition, Figure 4b shows pore radius change of Al_2O_3 ALD coated aerogels over various annealing temperatures (400 °C - 1000 °C). With the obtained experimental SAXS patterns by way of the SAXSGUI and MCSAS software, we determined the effective scattering radius, the mean particle, and the pore sizes of the interconnected particle network. We performed SAXS measurements of pristine and Al_2O_3 coated aerogels before and after annealing at various temperatures. Aerogel samples annealed at less than 600 °C showed pore radius changes less than 0.12 nm. On the other hand, noticeable pore radius change was observed in the samples annealed more than 800 °C, which agrees with the significant shrinkage of the samples as shown in Figure 4a. Therefore, these annealing studies demonstrated the enhanced thermal stability provided by Al_2O_3

ALD coatings on the silica aerogel. The more layers of Al_2O_3 ALD coating on silica aerogels, the less shrinkage and smaller pore radius change observed as shown in Figure 4a and 4b. The rate of change in pore radius increased with annealing temperature. On the other hand, the rate of change in pore radius changes decreased with more Al_2O_3 ALD coatings.

However, there exists a tradeoff since enhancing thermal stability via layering with the Al_2O_3 ALD coating compromises transmittance of the silica aerogel. Figure 4c shows direct-hemispherical transmittance (250 nm ~ 2500 nm) of aerogels with and without the Al_2O_3 ALD coating. The more layers coated, the less transmittance. The water affinity of both silica and alumina leads to water molecules bound to the surface of the samples, resulting in absorption peaks in Figure 4c. The inset of Figure 4d demonstrates that transmittance of Al_2O_3 ALD coated aerogels is inversely proportional to the number of ALD coatings. 25 and 100 layers of Al_2O_3 ALD coatings resulted in ~1.7 % and ~9.4 % decrease in transmittance, respectively. To gain insight into the decrease in transmittance, the optical cumulative loss rate (% / nm) was determined by differentiating spectral cumulative loss (%) across relevant wavelengths (nm). The optical cumulative loss was calculated as,

$$cummulative\ loss = \frac{\int_{250}^{\lambda} \mathrm{AM1.5}(\lambda)\, d\lambda \; - \int_{250}^{\lambda} \mathrm{AM1.5}(\lambda)\, \tau^{h}(\lambda) \mathrm{d}\lambda}{\int_{250}^{2500} \mathrm{AM1.5}(\lambda)\, \mathrm{d}\lambda}$$

where λ is wavelength (nm), AM 1.5 solar spectral irradiance at air mass 1.5, and τ^h is hemispherical transmittance. Both AM 1.5 and τ^h are a function of λ. The cumulative loss rate indicates that the majority of optical attenuation is due to scattering as shown in Figure 4d. While adsorption is the dominant extinction mechanism for longer wavelengths (> ~1200 nm), scattering is the dominant one for shorter wavelengths (< ~1200 nm, visible and UV). The cumulative loss rates peak at wavelengths less than 1000 nm, and therefore indicating the dominance of scattering.

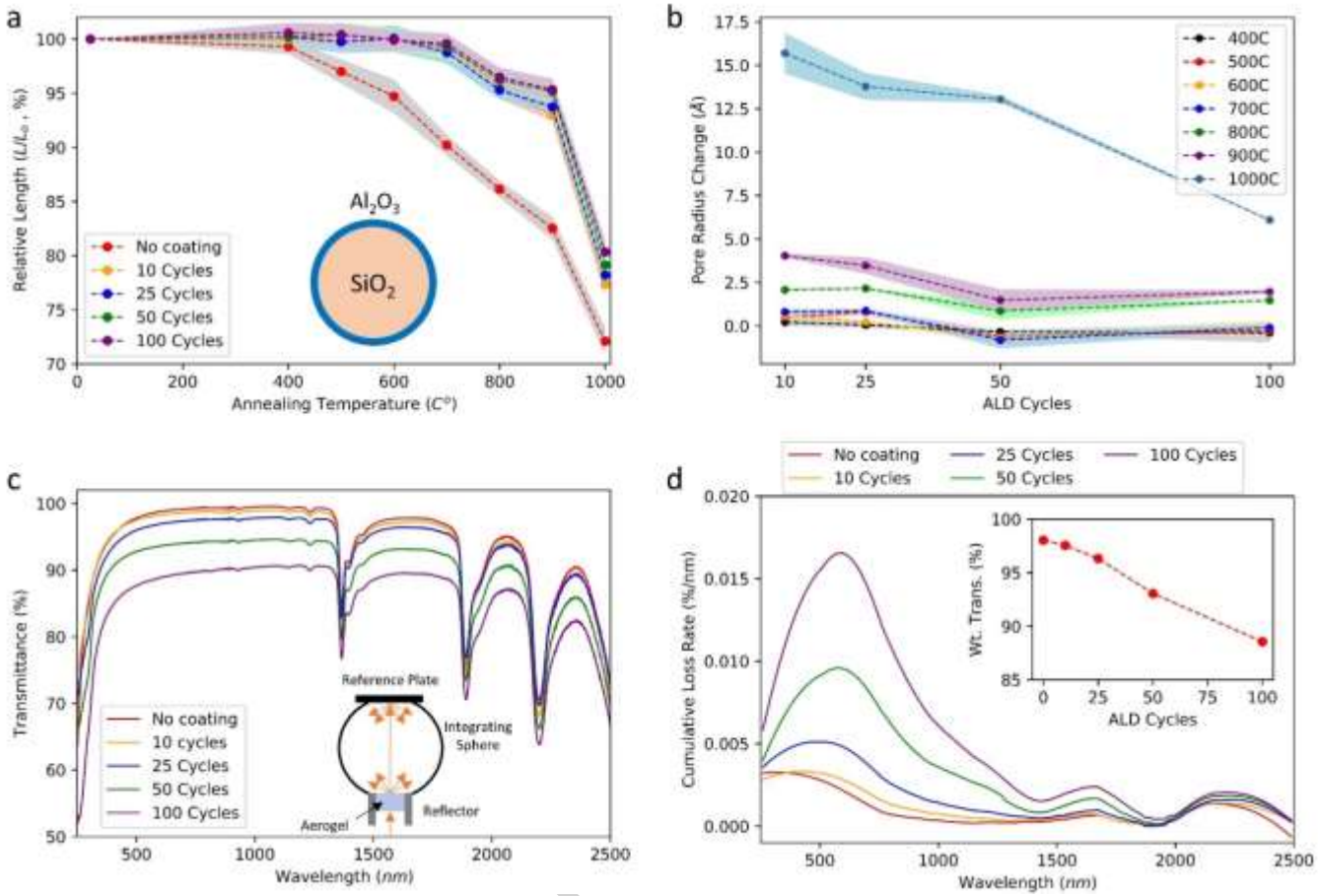

Figure 4. (a) Relative length of shrinkage of the aerogel with and without Al_2O_3 ALD coatings (0, 10, 25, 50 and 100 ALD cycles in red, yellow, blue, green and purple, respectively) as annealed between 400 and 1000 °C for 14 days. Direct measurement of the area of each sample was used to estimate length changes between different annealing temperatures. (b) Pore radius changes of aerogel with and without Al_2O_3 ALD coatings as annealed at various temperatures (400, 500, 600, 700, 800, 900 and 1000 °C in black, red, yellow, blue, green, purple, and light-blue, respectively). (c) Spectral transmission (250 ~ 2500 nm) of transparent aerogels with and without Al_2O_3 ALD coatings (0, 10, 25, 50 and 100 ALD cycles in red, yellow, blue, green and purple, respectively). The more ALD coating, the less transparent. (d) Spectral cumulative loss rate (250 ~ 2500 nm) of transparent aerogels with and without Al_2O_3 ALD coatings (0, 10, 25, 50 and 100 ALD cycles in red, yellow, blue, green and purple, respectively). The peaks of the cumulative loss rate lines show a redshift indicating an increase in scattering diameter. The inset shows the solar weighted transmittance of the transparent aerogel with and without Al_2O_3 ALD coatings.

As the layers of Al_2O_3 ALD coating increasesd the peak of the accumulative loss rate shifted toward longer wavelengths. Rayleigh-Gans theory states that the scattering coefficient is proportional to a diameter of the scattering center to the 3rd power. Therefore, the accumulative loss rate shifting toward longer wavelengths with increased the number of Al_2O_3 ALD coating can be attributed to the increase in particle size after the coating.

Despite the slightly increased optical loss (*i.e.*, 1.7 % decrease after 25 cycles of ALD coating on 3 mm thickness aerogel) in the solar spectrum, high temperature stable silica aerogels can enable a CSP system to operate efficiently at elevated temperatures (>600 °C) which make them compatible with high-efficiency power cycles, such as supercritical CO_2 (sCO_2) Brayton cycle. Compared with conventional steam cycles, sCO_2 cycle can achieve more than 50% power conversion efficiency, which holds great promise to improve the overall efficiency of a CSP system.[23–26] Currently, achieving high temperature in a CSP system relies on high optical concentration (>1000 suns) due to the increased heat loss. With the developed thermally stable silica aerogels, the heat loss can be significantly reduced to allow the use of low-cost optical concentration systems. We expect superior high temperature thermal stability utilizing zirconium (ZrO_2) or hafnium oxide (HfO_2) thin film coating which have melting temperatures higher than that of alumina oxide.[27,28] While economic viability, high energy waste rate and the limited scalability of ALD coating on OTTI aerogel could become a bottleneck,[29] the demonstrated ALD-coated OTTI aerogel provides a potential pathway to further improve the efficiency and reduce the cost of state-of-the-art CSP systems.

4. CONCLUSIONS

We investigated the effects of Al_2O_3 ALD coating on the thermal stability of silica aerogel. Al_2O_3 ALD coating enhanced thermal stability of silica aerogel. On the other hand, silica aerogels with Al_2O_3 ALD coating showed noticeable shrinkage after 600 ºC while silica aerogels without Al_2O_3 coating shrunk after ~400 ºC. After 25 cycles of Al_2O_3 ALD coating, transmittance of silica aerogel decreased only 1.7 % from 98.0 % at 3 mm sample thickness. The more layers of Al_2O_3 ALD coating, the less shrinkage observed however compromising optical transmittance of the samples. As the performance of solar thermal system is a function of both transmittance of silica aerogel and operating temperature, the optimization of Al_2O_3 ALD on transparent silica aerogels need to balance transmission and thermal properties. This work provides insights for a potential pathway to further improve the efficiency and reduce the cost of state-of-the-art CSP systems and the development of high temperature stable transparent insulation in various solar thermal applications.

ACKNOWLEDGEMENTS

This work was supported by the ARPA-E FOCUS program (DE-AR0000471) and MIT Center for Materials Science and Engineering (CMSE).

DECLARATION OF COMPETING INTEREST

The authors declare that they have no known competing financial interests or personal relationships that could have appeared to influence the work reported in this paper.

REFERENCES

(1) Crabtree, G. W.; Lewis, N. S. Solar Energy Conversion. *Phys. Today* **2007**, *60* (3), 37–42. https://doi.org/10.1063/1.2718755.

(2) Weinstein, L. A.; Loomis, J.; Bhatia, B.; Bierman, D. M.; Wang, E. N.; Chen, G. Concentrating Solar Power. *Chem. Rev.* **2015**, *115* (23), 12797–12838. https://doi.org/10.1021/acs.chemrev.5b00397.

(3) Iverson, B. D.; Conboy, T. M.; Pasch, J. J.; Kruizenga, A. M. Supercritical CO2 Brayton Cycles for Solar-Thermal Energy. *Appl. Energy* **2013**, *111*, 957–970. https://doi.org/10.1016/j.apenergy.2013.06.020.

(4) Svendsen, S. Solar Collector with Monolithic Silica Aerogel. *J. Non-Cryst. Solids* **1992**, *145*, 240–243. https://doi.org/10.1016/S0022-3093(05)80464-8.

(5) Haranath, D.; Pajonk, G. M.; Wagh, P. B.; Rao, A. V. Effect of Sol-Gel Processing Parameters on Thermal Properties of Silica Aerogels. *Mater. Chem. Phys.* **1997**, *49* (2), 129–134. https://doi.org/10.1016/S0254-0584(96)01924-4.

(6) McEnaney, K.; Weinstein, L.; Kraemer, D.; Ghasemi, H.; Chen, G. Aerogel-Based Solar Thermal Receivers. *Nano Energy* **2017**, *40*, 180–186. https://doi.org/10.1016/j.nanoen.2017.08.006.

(7) Weinstein, L. A.; McEnaney, K.; Strobach, E.; Yang, S.; Bhatia, B.; Zhao, L.; Huang, Y.; Loomis, J.; Cao, F.; Boriskina, S. V.; Ren, Z.; Wang, E. N.; Chen, G. A Hybrid Electric and Thermal Solar Receiver. *Joule* **2018**, *2* (5), 962–975. https://doi.org/10.1016/j.joule.2018.02.009.

(8) Optically Transparent Thermally Insulating Silica Aerogels for Solar Thermal Insulation | ACS Applied Materials & Interfaces https://pubs.acs.org/doi/10.1021/acsami.7b18856 (accessed Jun 27, 2021).

(9) Berardi, U. Development of Glazing Systems with Silica Aerogel. *Energy Procedia* **2015**, *78*, 394–399. https://doi.org/10.1016/j.egypro.2015.11.682.

(10) Buratti, C.; Moretti, E.; Zinzi, M. High Energy-Efficient Windows with Silica Aerogel for Building Refurbishment: Experimental Characterization and Preliminary Simulations in Different Climate Conditions. *Buildings* **2017**, *7* (1), 8. https://doi.org/10.3390/buildings7010008.

(11) Brinker, C. J.; Scherer, G. W.; Roth, E. P. Sol → Gel → Glass: II. Physical and Structural Evolution during Constant Heating Rate Experiments. *J. Non-Cryst. Solids* **1985**, *72* (2), 345–368. https://doi.org/10.1016/0022-3093(85)90189-9.

(12) Christensen, R. M. Relaxation in Glass and Composites. By G. W. Sherer, John Wiley & Sons, 1986, 331 Pp. *AIChE J.* **1987**, *33* (6), 1053–1054. https://doi.org/10.1002/aic.690330625.

(13) Strobach, E.; Bhatia, B.; Yang, S.; Zhao, L.; Wang, E. N. High Temperature Stability of Transparent Silica Aerogels for Solar Thermal Applications. *APL Mater.* **2019**, *7* (8), 081104. https://doi.org/10.1063/1.5109433.

(14) Harnessing Heat Beyond 200 °C from Unconcentrated Sunlight with Nonevacuated Transparent Aerogels | ACS Nano https://pubs.acs.org/doi/10.1021/acsnano.9b02976 (accessed Aug 9, 2020).

(15) Abramoff, M. D.; Magalhães, P. J.; Ram, S. J. Image Processing with ImageJ. *Biophotonics Int.* **2004**, *11* (7), 36–42.

(16) Bressler, I.; Pauw, B. R.; Thünemann, A. F. McSAS: Software for the Retrieval of Model Parameter Distributions from Scattering Patterns. *J. Appl. Crystallogr.* **2015**, *48* (3), 962–969. https://doi.org/10.1107/S1600576715007347.

(17) Cleveland IV, T.; Blick, E.; Krueger, S.; Leung, A.; Darwish, T.; Butler, P. Direct Localization of Detergents and Bacteriorhodopsin in the Lipidic Cubic Phase by Small-Angle Neutron Scattering. *IUCrJ* **2021**, *8* (1), 22–32. https://doi.org/10.1107/S2052252520013974.

(18) Zhao, L.; Yang, S.; Bhatia, B.; Strobach, E.; Wang, E. N. Modeling Silica Aerogel Optical Performance by Determining Its Radiative Properties. *AIP Adv.* **2016**, *6* (2), 025123. https://doi.org/10.1063/1.4943215.
(19) Brinker, C. J.; Scherer, G. W. CHAPTER 5 - Gelation. In *Sol-Gel Science*; Brinker, C. J., Scherer, G. W., Eds.; Academic Press: San Diego, 1990; pp 302–355. https://doi.org/10.1016/B978-0-08-057103-4.50010-6.
(20) Quinson, J. F.; Tchipkam, N.; Dumas, J.; Bovier, C.; Serughetti, J.; Guizard, C.; Larbot, A.; Cot, L. Swelling of Titania Gels in Decane. *J. Non-Cryst. Solids* **1988**, *99* (1), 151–159. https://doi.org/10.1016/0022-3093(88)90467-X.
(21) Brinker, C. J.; Scherer, G. W. CHAPTER 6 - Aging of Gels. In *Sol-Gel Science*; Brinker, C. J., Scherer, G. W., Eds.; Academic Press: San Diego, 1990; pp 356–405. https://doi.org/10.1016/B978-0-08-057103-4.50011-8.
(22) Wang, Z.-Y.; Zhang, R.-J.; Lu, H.-L.; Chen, X.; Sun, Y.; Zhang, Y.; Wei, Y.-F.; Xu, J.-P.; Wang, S.-Y.; Zheng, Y.-X.; Chen, L.-Y. The Impact of Thickness and Thermal Annealing on Refractive Index for Aluminum Oxide Thin Films Deposited by Atomic Layer Deposition. *Nanoscale Res. Lett.* **2015**, *10* (1), 46. https://doi.org/10.1186/s11671-015-0757-y.
(23) Ahn, Y.; Bae, S. J.; Kim, M.; Cho, S. K.; Baik, S.; Lee, J. I.; Cha, J. E. Review of Supercritical CO2 Power Cycle Technology and Current Status of Research and Development. *Nucl. Eng. Technol.* **2015**, *47* (6), 647–661. https://doi.org/10.1016/j.net.2015.06.009.
(24) Crespi, F.; Gavagnin, G.; Sánchez, D.; Martínez, G. S. Supercritical Carbon Dioxide Cycles for Power Generation: A Review. *Appl. Energy* **2017**, *195*, 152–183. https://doi.org/10.1016/j.apenergy.2017.02.048.
(25) Li, M.-J.; Zhu, H.-H.; Guo, J.-Q.; Wang, K.; Tao, W.-Q. The Development Technology and Applications of Supercritical CO2 Power Cycle in Nuclear Energy, Solar Energy and Other Energy Industries. *Appl. Therm. Eng.* **2017**, *126*, 255–275. https://doi.org/10.1016/j.applthermaleng.2017.07.173.
(26) Neises, T.; Turchi, C. A Comparison of Supercritical Carbon Dioxide Power Cycle Configurations with an Emphasis on CSP Applications. *Energy Procedia* **2014**, *49*, 1187–1196. https://doi.org/10.1016/j.egypro.2014.03.128.
(27) Arpin, K. A.; Losego, M. D.; Cloud, A. N.; Ning, H.; Mallek, J.; Sergeant, N. P.; Zhu, L.; Yu, Z.; Kalanyan, B.; Parsons, G. N.; Girolami, G. S.; Abelson, J. R.; Fan, S.; Braun, P. V. Three-Dimensional Self-Assembled Photonic Crystals with High Temperature Stability for Thermal Emission Modification. *Nat. Commun.* **2013**, *4* (1), 2630. https://doi.org/10.1038/ncomms3630.
(28) Chang, I.; Lee, J.; Lee, Y.; Lee, Y. H.; Ko, S. H.; Cha, S. W. Thermally Stable Ag@ZrO2 Core-Shell via Atomic Layer Deposition. *Mater. Lett.* **2017**, *188*, 372–374. https://doi.org/10.1016/j.matlet.2016.11.105.
(29) Johnson, R. W.; Hultqvist, A.; Bent, S. F. A Brief Review of Atomic Layer Deposition: From Fundamentals to Applications. *Mater. Today* **2014**, *17* (5), 236–246. https://doi.org/10.1016/j.mattod.2014.04.026.